Impact of Head Group Charges, Ionic Sizes, and Dielectric Images on Charge Inversion: A Monte Carlo Simulation Study

ARTICLE *in* THE JOURNAL OF PHYSICAL CHEMISTRY B · OCTOBER 2010

Impact Factor: 3.3 · DOI: 10.1021/jp106118q · Source: PubMed

2 AUTHORS, INCLUDING:

Zhi Yong Wang
Chongqing University of Technology
21 PUBLICATIONS **187** CITATIONS

Impact of Head Group Charges, Ionic Sizes, and Dielectric Images on Charge Inversion: A Monte Carlo Simulation Study

Zhi-yong Wang[†,‡] **and Yu-qiang Ma***[,‡,§]

School of Optoelectronic Information, Chongqing University of Technology, Chongqing 400054, China, National Laboratory of Solid State Microstructures and Department of Physics, Nanjing University, Nanjing 210093, China, and Laboratory of Soft Condensed Matter Physics and Interdisciplinary Research, Soochow University, Suzhou 215006, China

Received: July 2, 2010; Revised Manuscript Received: September 6, 2010

The ionic density profiles and corresponding integrated charge distribution close to an aqueous interface carrying charged functional groups of different valences exposed to mixed-salt solutions of 1:1 and 3:1 electrolytes were computed by use of extensive Monte Carlo simulations within the framework of the primitive model. The influence of varying ion sizes on charge inversion was analyzed, along with the crucial role of electrostatic images arising from dielectric discontinuities. For small sizes of charged species, it was found that charge inversion is enhanced by the presence of multivalent interfacial groups. Moreover, dielectric images further intensify the degree of charge inversion despite strong depletion effects. In particular, the onset of charge inversion shifts closer to the nonaqueous phase if the surface charge density is sufficiently low. These observations are opposite to the general belief of image repulsion. When large-sized ions were considered, the degree of charge inversion was found to be independent of the structure of interfacial groups and to remain widely unaffected in the absence and presence of dielectric images. Overall, our results show that interionic excluded-volume interactions are an overwhelming factor in determining counterion condensation. In addition, the inclusion of ionic size asymmetry at weakly charged interface results in surface charge amplification, which becomes more pronounced with increasing valence of the interfacial groups. Our work emphasizes the fact that surface equilibria mainly result from a subtle balance between steric and charge correlations.

I. Introduction

The general problem of an interface between two phases that are charged is of relevance to a number of systems appearing ubiquitously in soft matter and biophysics. This ensures that electrostatic interactions play a fundamental role in a plethora of important physicochemical, biological, and technological processes.[1,2] Typically, a charged particle immersed in an electrolyte solution tends to be surrounded by opposite charges, some of which are bound while others are mobile. This characteristic structure is commonly referred to as the electric double layer (EDL),[3] which pervades the entire realm of interface and colloid science at phase boundaries. Moreover, the electrostatics in complex fluids usually exhibits nonintuitive phenomena such as charge inversion.[4,5] This fascinating effect consists in the binding of counterions in excess of the native charge of the interface, thus resulting in a dressed interface whose effective charge changes sign. Various explanations have been put forward as to the mechanisms of charge inversion.[6−15] In particular, charge inversion has been shown both theoretically and experimentally to be related to attractive interactions between like-charged macroions in the presence of polyvalent counterions where ion−ion correlation effects become dominantly important.[13−25] Hence, it has implications for drug delivery[26−28] and for the understanding of new discoveries related to assemblies of charged nanoparticles with biomolecules, as well as their interactions with cells.[29−32]

A well-known example associated with the EDL is a planar layer of phospholipid molecules with charged head groups in contact with an electrolyte solution. Depending on the charges of additional groups that might be bound to the phosphate groups, phospholipids in aqueous medium can have a valency in the range between −4 and +1 under physiological conditions.[33−36] Normally, the standard theoretical approach for describing the distribution of ions in solution adjacent to a charged interface has been the Poisson−Boltzmann (PB) theory under the simplifying assumptions that the interface has a uniformly smeared out distribution of charge and that all correlations among mobile ions are neglected. Over the past decade, however, combined theoretical and experimental works have explicitly pointed out that these two assumptions are too simplistic for achieving a more realistic description of the interactions of charged macromolecules in biological and soft condensed matter systems.[12−15] More recently, Fleck et al. employing a corrected PB theory showed that the mobility of interfacial head groups can lead to the adsorption of negatively charged DNA onto a like-charged membrane.[37] Based on molecular dynamics simulations, Calero and Faraudo suggested that charge inversion is enhanced by multivalent interfacial groups in contact with a 2:1 ionic solution for $\sigma_0 = -0.9e/\mathrm{nm}^2$.[38] In a separate article, these authors further showed that the electrostatic potential depends strongly on the valence of interfacial charged groups.[39]

A further point to consider, when studying biological macromolecules and macromolecular structures, is the disparity between the permittivities inside and outside them. This

* Corresponding author. E-mail: myqiang@nju.edu.cn.
† Chongqing University of Technology.
‡ Nanjing University.
§ Soochow University.

10.1021/jp106118q
Published on Web 10/06/2010

dielectric effect is usually described in terms of so-called image charges, which play a crucial role in the ion filtration mechanism regulating ion flow through cell membranes and ensuring ion selectivity in biological channels.[40−42] In an early work, Torrie et al. reported that the effect of image charges can be quite large at low surface charge densities and gradually decreases with increasing surface charge.[43] A similar conclusion was drawn by our recent work for models with different surface charge distributions.[44] Moreover, we also revealed that, in the strong-Coulomb-coupling regime, charge inversion is independent of dielectric images even if the surface charges are discretely positioned on a regular square network of monovalent charged sites. For a more realistic picture, Henderson et al. specially introduced a region adjacent to the uncharged interface, known as the Stern layer, where the dielectric constant is different from those of the solvent and the dielectric substrate.[45] They found that, if the Stern layer is sufficiently large, the dielectric constant of this layer governs the distribution of the ions, rather than the dielectric constant of the dielectric substrate.

The above discussion begs that the question of what level of theory is required to capture the essential physical effects on charge inversion of charged interfaces. The purpose of the current study is to provide further numerical justification aimed at understanding the combined effects of polyvalent interfacial groups, ion size, and dielectric images on this peculiar phenomenon. Two typical surface charge densities were chosen to represent systems from weak to strong electrostatic coupling. Resorting to an extensive series of Monte Carlo simulations in the framework of the primitive model, we investigated a negatively charged planar dielectric interface bearing uniformly distributed fixed charges exposed to an aqueous solution containing a mixture of 1:1 and 3:1 electrolytes, where the monovalent salt was used to characterize physiological conditions. Such a discrete representation of surface charges over a continuous one employing surface charge densities allowed us to simultaneously take the charge and steric correlations into account.

This article is structured as follows: In section II, we provide a brief description of the simulation approach and the details of the model system. In section III, we present and discuss the general properties of supporting charge inversion corresponding to this model. Finally, we provide some concluding remarks in section IV.

II. Model and Simulation Procedure

Our simulations were carried out within the framework of the primitive model of mixed electrolytes, in which the ions are represented by hard spheres of different diameters with point charges at their centers. Aqueous and nonaqueous media are characterized as dielectric continua defined exclusively by their respective permittivities and separated from each other by an infinitely sharp and perfectly flat interface carrying fixed charges that are assumed to result from a dissociation of ionizable groups. They are arranged in a square lattice and treated as hard spheres with a finite diameter of 6 Å whose centers are situated just on the interface. The effect of explicit interfacial groups was analyzed in terms of head groups of different valencies $Z_h \in \{-1, -2, -3, -4\}$.[33−36] For the choice of surface charge density, we used the two experimentally relevant values of -0.04 and -0.24 C/m^2,[46] which correspond to different site-to-site separations when created by a regular square network of interfacial groups under study. In terms of a given surface charge density, the higher the valency of head groups on the interface, the larger the site-to-site separation.

The simulation cell was a rectangular prism of dimensions $W \times W \times 2L$, taken to be periodic in the horizontal (x and y) directions, and finite in the vertical (z) direction. Two impenetrable walls of the cell were uncharged and were located at $z = \pm L$. For symmetry, a third impenetrable wall was positioned at $z = 0$ and represented a biological interface between two different dielectric phases. All mobile ionic species were confined to the aqueous environment at $z > 0$. Moreover, we assumed that the interior of the ions had the same dielectric constant as the surrounding medium.

The electrostatic energy of a single electrolyte ion i due to the interfacial group k can be written in the form

$$U^{\mathrm{one}}(r_{ik}) = (1 + \Delta_\epsilon)\frac{Z_i Z_k e^2}{4\pi\epsilon_0\epsilon_> r_{ik}} \tag{1}$$

where Z_i is the valency of charges of type i, r_{ik} is the center-to-center distance, and e is the positive elementary charge. ϵ_0 and $\epsilon_>$ are the permittivity of the vacuum and the dielectric constant of the aqueous solvent, respectively. The factor Δ_ϵ characterizing the dielectric jump is given by $\Delta_\epsilon = (\epsilon_> - \epsilon_<)/(\epsilon_> + \epsilon_<)$, where $\epsilon_<$ represents the relative permittivity of the nonaqueous medium. In addition, the electrostatic energy of the ion i due to its image charge is given by

$$U^{\mathrm{self}}(z_i) = \frac{Z_i^2 \Delta_\epsilon e^2}{16\pi\epsilon_0\epsilon_> z_i} \tag{2}$$

Each two electrolyte ions i and j with a spatial separation distance of $r_{ij} \geqslant (d_i + d_j)/2$ (where d_i is the diameter of ionic species i) contributes to the electrostatic potential energy simply by the ordinary Coulomb potential

$$U^{\mathrm{two}}(r_{ij}) = \frac{Z_i Z_j e^2}{4\pi\epsilon_0\epsilon_>}\left(\frac{1}{r_{ij}} + \frac{\Delta_\epsilon}{\sqrt{r_{ij}^2 + 4z_i z_j}}\right) \tag{3}$$

The second term in eq 3 denotes the mutual interaction between the source charge i and the image of charge j. Coulomb collapse can be eliminated by the inclusion of a short-range hard-core overlap restriction among all the charges

$$U^{\mathrm{hs}}(r_{ij}) = \begin{cases} \infty & \text{if } r_{ij} < (d_i + d_j)/2 \\ 0 & \text{otherwise} \end{cases} \tag{4}$$

A one-body external field was imposed to maintain all mobile species inside the aqueous environment, so that

$$U^{\mathrm{ex}}(z_i) = \begin{cases} \infty & \text{if } z_i < d_i/2 \text{ or } z_i > L - d_i/2 \\ 0 & \text{otherwise} \end{cases} \tag{5}$$

Taken together, the total potential energy of interaction in our calculations is given by

$$U^{\text{tot}} = \sum_{i}^{N}\sum_{k}^{M}[U^{\text{one}}(r_{ik}) + U^{\text{hs}}(r_{ik})] + \sum_{i}^{N}\sum_{i<j}^{N}[U^{\text{two}}(r_{ij}) + U^{\text{hs}}(r_{ij})] + \sum_{i}^{N}[U^{\text{self}}(z_i) + U^{\text{ex}}(z_i)] \quad (6)$$

where M and N are the total numbers of interfacial groups and mobile ions, respectively.

To explore the system configuration space, standard Metropolis Monte Carlo sampling simulations[47] were carried out in the canonical (*NVT*) ensemble. The long-range nature of the Coulomb interaction requires the use of periodic images to properly account for the electrostatics. Because the system under study was periodic in only the x and y directions, and not in z direction, we employed a recently modified Lekner summation method[48] that can efficiently deal with the slab geometry of present interest. All calculations throughout the current article were performed with a relative dielectric permittivity of $\epsilon_> = 78.5$ corresponding to water at room temperature of 298 K. To investigate the effect of image charges, we considered a typical value of $\epsilon_< = 2$ for the dielectric interior within biomembranes. At the same time, we also performed further simulations by neglecting the dielectric discontinuities (i.e., $\epsilon_> = \epsilon_< = 78.5$) for comparison and completeness. To include the effect of the ion size on the charge reversal process, calculations were performed for both the restricted and unrestricted primitive models, which we abbreviate as RPM and UPM, respectively, for convenience. In the RPM representation of electrolytes, all of the ions are assumed to have a uniform diameter of 4 Å. This value has been used extensively in the theoretical treatment of electrolyte solutions.[14] For the UPM approximation, we assumed that all monovalent species have an identical hydrated diameter of 7.2 Å.[44] However, the diameter of the trivalent counterions was taken as 9.6 Å.[44] It should be mentioned that the UPM offers an advantage over the RPM representation: The ion size asymmetry is included, and thus, the UPM is a step closer to real salt solutions. For all cases, the concentrations of monovalent and trivalent salts were both fixed at 100 mM. Depending on the size of the simulation cell, the total number N of electrolyte ions varied between 800 and 2500, chosen in such a way that the co-ions and counterions exactly balanced the interfacial charges. Each simulation started from a random initial configuration satisfying the combined constraints of eqs 4 and 5. Typically, after an equilibration period greater than 8×10^4 cycles, the physical quantities of interest were calculated during the next more 4×10^5 cycles. During this production period, results were recorded every 8−12 cycles from one simulation to another for data analysis purposes. One cycle corresponds to N translation attempts in a random fashion. The acceptance rate was kept between 0.4 and 0.5 by automatically adjusting the step length to move individual ion coordinates. It was verified that the simulation cell was large enough to circumvent spurious periodic-image effects.

III. Results and Discussion

Central to this work was the calculation of the density profiles of all ionic species $\rho_l(z)$ with $l \in \{-1, +1, +3\}$ through the use of a standard histogram procedure. Such profiles can provide evidence about the possible existence of charge inversion. It should be pointed out that, for the discrete surface charges considered here, the ionic local densities are not homogeneous but depend on all three directions. However, in the present work, we concentrate only on the distribution in the z direction perpendicular to the membrane surface. Therefore, our data might be interpreted as laterally averaged values over the x and y directions parallel to the interface. Once the $\rho_l(z)$ profiles are available, charge inversion can be better revealed by the integrated charge distribution function, $\sigma_{\text{int}}(z)$, which is defined as

$$\sigma_{\text{int}}(z) = \sigma_0 + \int_0^z \mathrm{d}z' \sum_{l=-1,+1,+3} Z_l e \rho_l(z') \quad (7)$$

where σ_0 is the bare surface charge density. $\sigma_{\text{int}}(z)$ represents the total charge "seen" at a distance z from the surface, including the charge of the surface itself plus the charge density of the double layer integrated from the surface to the distance z. More generally, charge inversion occurs once $\sigma_{\text{int}}(z)$ induces a reversal in the surface polarity. In any case, $\sigma_{\text{int}}(z)$ goes to zero when $z \to \infty$ to satisfy the overall electroneutrality condition.

A. Charge Inversion in Weak Electrostatic Coupling Systems. We first consider the microscopic structure of the EDL in terms of the distribution of electrolyte ions near a weakly charged surface of $\sigma_0 = -0.04$ C/m^2. Figures 1 and 2 present the density profiles of all ionic species for different values of the charge of the interfacial groups within the scope of the RPM and UPM representations, respectively, in the absence and presence of dielectric images. The profiles for all three solution components were normalized relative to the corresponding bulk densities obtained by averaging the density distribution in the middle part of the aqueous phase where the bulk fluid was uniform. Thus, it is clear that the normalized values are all unity at distances far from the membrane surface. Without loss of generality, the oppositely charged counterions in the solution concentrate in the vicinity of the interface, whereas the like-charged co-ions are depleted as a result of the electrostatic interactions. Moreover, the surface charges can be preferentially screened by trivalent counterions for their stronger attraction than monovalent ones. The rise of the valence of interfacial

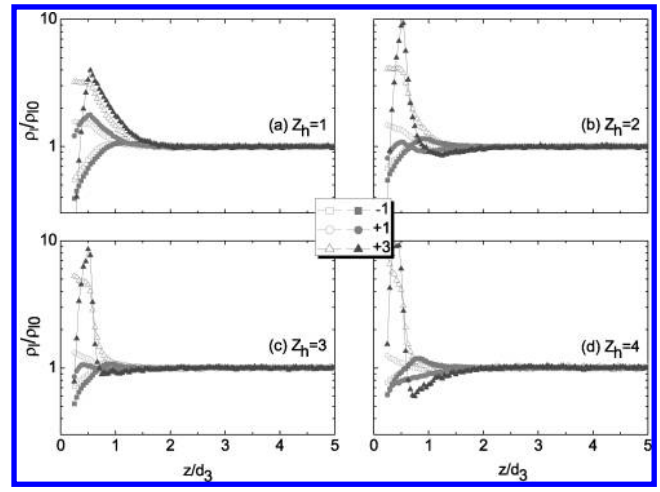

Figure 1. Normalized density profiles of ions averaged over the x and y directions as a function of the distance (rescaled by dividing by $d_3 = 9.6$ Å) to a charged surface of $\sigma_0 = -0.04$ C/m^2 in contact with a mixture of 1:1 and 3:1 electrolytes both with the same bulk contents of 100 mM for the interfacial groups of different valences, Z_h = (a) 1, (b) 2, (c) 3, and (d) 4. All ionic diameters are assumed to be 4 Å in the RPM representation of electrolytes. Squares, circles, and triangles represent co-ions, monovalent counterions, and trivalent counterions, respectively. The open and solid symbols represent the results in the absence and presence of dielectric images, respectively.

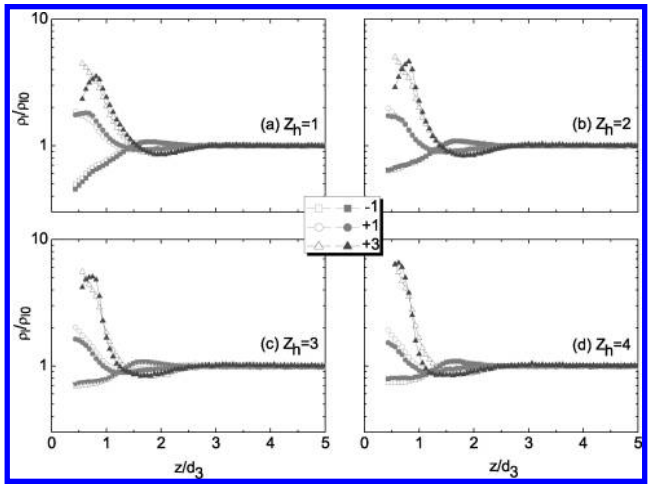

Figure 2. Same as Figure 1 but for the UPM representation of electrolytes, in which all monovalent species are assumed to have the same hydrated diameter of 7.2 Å and the diameter of trivalent counterions is assumed to be 9.6 Å. All other parameters are the same as in Figure 1.

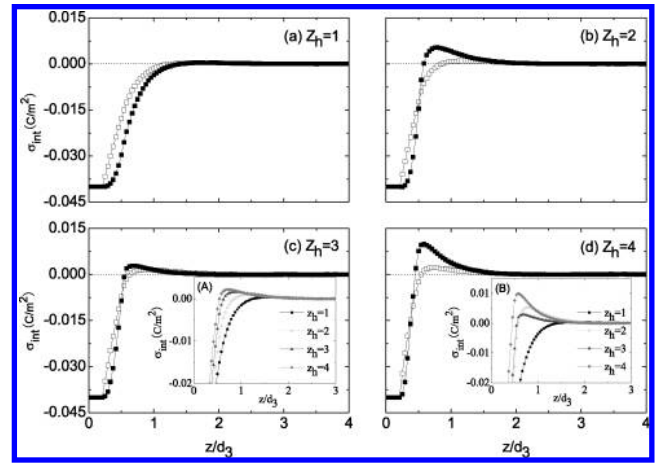

Figure 3. Integrated charge profiles plotted as a function of the dimensionless distance to the surface within the framework of the RPM approximation. All parameters are the same as in Figure 1. Open and solid symbols represent the results in the absence and presence of dielectric images, respectively. Insets: Magnification of integrated charge at small values of interfacial distance for varying valence of the head groups in the (A) absence and (B) presence of dielectric images.

groups causes more accumulation of trivalent counterions and monovalent co-ions nearer the membrane surface. This is because the ions associate to form charged clusters that can be attached together to the interface. In contrast, the amount of monovalent counterions decreases. The situation is more appreciable for the RPM systems under investigation. It can also be seen that the impact of repulsive image forces on the structure of the double layer is quite large for small ions to create a local maximum slightly away from the contact layer, especially in the profile of trivalent counterions. This behavior has significant implications for colloid stability, where a component of the force between two colloid particles is intimately related to the ionic densities around the surface. On the other hand, the effect of images is strikingly impaired for large ions.

We can further see from Figure 1 that all of the ionic profiles are monotonic for $Z_h = 1$ in the absence of image charges. More explicitly, these functions are increasing for co-ions and decreasing for monovalent and trivalent counterions. By contrast, Figure 2a shows that the counterion density curves display a minimum adjacent to the surface, whereas the co-ion profile assumes a maximum almost at the same position. The nonlinear PB equation fails to account for this feature because it always predicts monotonic variations for the density profiles of both co-ions and counterions. In our case, however there is a layer just outside the surface with a net charge of sign opposite to that of σ_0 followed by a layer with the same sign as σ_0. The number of counterions in the neighborhood of the interface then overcompensates the amount needed to neutralize the bare surface charges, giving rise to the phenomenon of charge inversion. Obviously, this effect is purely attributed to the significance of the excluded-volume correlations, similar to what was observed for a uniformly smeared charged interface.[11,49] When the charges of the head groups on the membrane are greater than 2, Figures 1 and 2 jointly illustrate that charge inversion is ubiquitously present, indicating that. apart from steric correlations, the presence of multivalent interfacial groups is also a driving factor for charge inversion in systems with weak electrostatic coupling. Moreover, it is clearly seen that the thickness of the EDL depends substantially on the valence of the interfacial charged groups, as well as on the ionic size variations. The double layer becomes narrow and more compact at high values of valence, whereas at low values, it becomes broad and more diffused. At the same time, the larger the ionic size, the wider the double layer. These characteristics are irrelevant to whether the dielectric images are taken into account.

It is well-known that charge inversion consists in the excess accumulation of counterions in a region very close to the charged surface. To better illustrate the occurrence of such accumulation, in Figure 3, we plot the integrated charge profiles for different valences of head groups in the RPM approximation by considering the systems with and without dielectric images. It is first of all noticeable that the inclusion of image charges yields a dramatic depletion effect. Despite this fact, the onset of charge inversion still presents an obvious shift toward the surface rather than away from it for all cases of the multivalent interfacial groups considered here. Impressively, the presence of dielectric images even enhances the amount of charge inversion, as shown by the larger peak. Actually, this behavior can be initially recognized in Figure 1, where the density profile of trivalent counterions shows a stronger peak relative to the no-image case. This implies that dielectric discontinuities are more efficiently felt when charge correlations becomes important. However, for $Z_h = 1$, the situation becomes qualitatively different. One can see from Figure 3a that the integrated charge approaches zero monotonically as $z \rightarrow \infty$, showing that the surface charges are fully screened at distance much larger than the screening length. In addition, it is clear from the insets in Figure 3 that the position of the maximal value of the integrated charge shifts closer to the surface with the valence of interfacial groups because of the favorable electrostatic correlations between head groups and counterions. In particular, the magnitude of the overcompensated charge monotonically increases when no image charges are present. Our calculations are in agreement with the recent results from molecular dynamics simulations for single-salt solutions near a moderately charged surface.[38] Upon polarizing the charged interface, the monotonic behavior in the strength of charge inversion breaks down at $Z_h = 3$.

Figure 4 shows the same curves as Figure 3 but for the UPM representation of electrolyte solutions in which the important ionic size and size asymmetry have been simultaneously introduced for a more realistic consideration. It can be seen that the profile of $\sigma_{int}(z)$ overshoots unity and reaches its maximum value for all cases under study, indicating the appearance of charge inversion at these distances. At the low surface charge

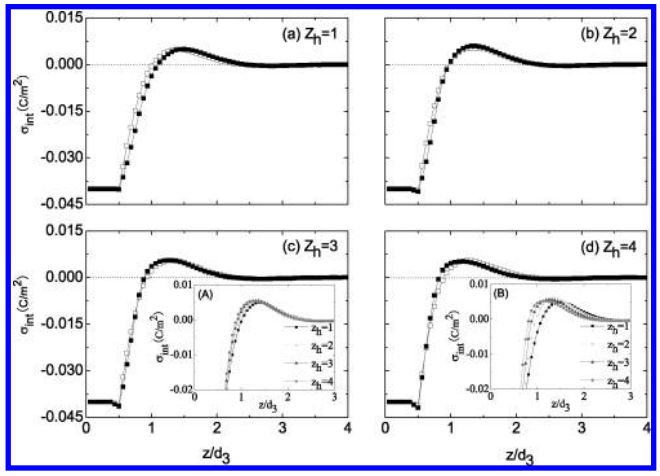

Figure 4. Same as Figure 3 but for the UPM systems. All parameters are the same as in Figure 2.

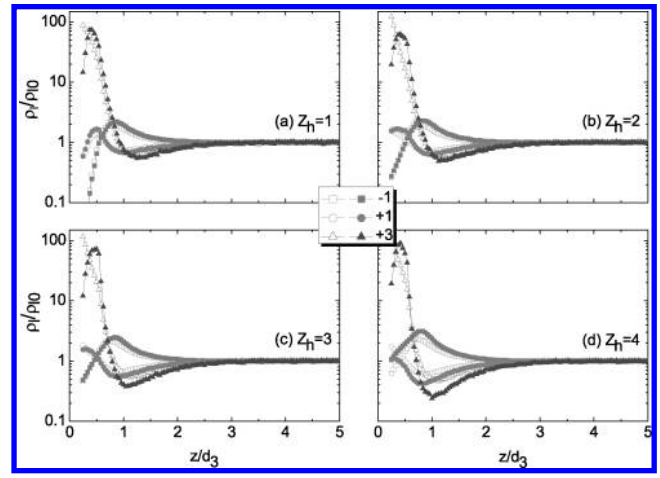

Figure 5. Normalized density profiles of ions averaged over the x and y directions as a function of the dimensionless distance near a charged surface with the surface charge density $\sigma_0 = -0.24$ C/m^2 in a mixed-salt solution of 100 mM monovalent and 100 mM trivalent electrolytes for varying charges of interfacial groups, Z_h = (a) 1, (b) 2, (c) 3, and (d) 4. All ionic diameters are assumed to be 4 Å in the RPM representation of electrolytes. Squares, circles, and triangles represent co-ions, monovalent counterions, and trivalent counterions, respectively. The open and solid symbols represent the results in the absence and presence of dielectric images, respectively.

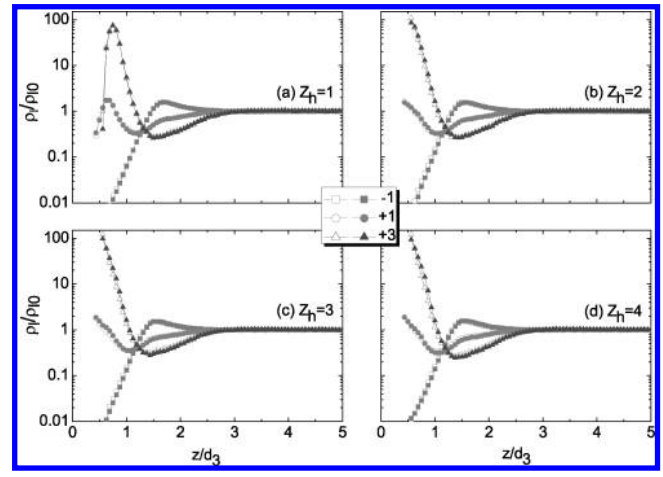

Figure 6. Same as Figure 5 but for the UPM representation of electrolytes, in which all monovalent species are assumed to have the same hydrated diameter of 7.2 Å and the diameter of trivalent counterions is assumed to be 9.6 Å. All other parameters are the same as in Figure 5.

density, an increase of the charge of interfacial groups again causes the onset of charge inversion in the presence of dielectric discontinuities to be closer to the surface than in the case of the absence of image charges, contrary to the general belief of dielectric repulsion. It should be pointed out that the effect has been evidently weakened as compared to RPM systems, as shown in Figure 3, where small ionic sizes are used. Interestingly, the proper inclusion of the size asymmetry of ions at this weakly charged interface results in surface charge amplification from adsorption of charge of the same polarity that is gradually enhanced with the charge of interfacial groups but little affected by the presence of dielectric images. This peculiar phenomenon has been reported in the most recent literature[44,49,50] and is expected to occur at high bulk concentrations of multivalent electrolyte. Our present findings further enrich the nonintuitive behavior. Additionally, as shown in the insets of Figure 4, the onset of charge inversion is still sensitive to the charges of interfacial groups. Specifically speaking, the appearance of charge inversion shifts nearer to the surface with the increase of the valence of head groups, similar to the RPM systems. However, the height in the integrated charge profiles remains widely unaffected for all cases in the absence and presence of dielectric jump. The feature is completely different from the RPM approximation of the small size of ions, where the coupling of both dielectric images and multivalent interfacial groups can intensify charge inversion. In particular, when $Z_h = 4$, the peak height of the $\sigma_{int}(z)$ curve is even larger in the RPM than in the UPM, just as will also be observed below for the highly charged surface. This trend of variation is opposite to the case of surface charge continuous distribution where the excluded-volume interactions are believed to always play a favorable role in the magnitude of charge inversion,[49] revealing the significance of the structural nature of interfacial charges.

B. Charge Inversion in Strong Electrostatic Coupling Systems. In Figures 5 and 6, we present the normalized density profiles of various components relative to their bulk values next to a strongly charged surface with $\sigma_0 = -0.24$ C/m^2 immersed in a mixture of 100 mM monovalent and 100 mM trivalent salts by varying charges of interfacial groups within the framework of the RPM and UPM approximations, respectively. As before, all curves were averaged over the x and y directions. Figures 5 and 6 show that, in comparison with the weak electrostatic coupling systems, there is a more significant accumulation of counterions near the highly charged surface, accompanied by a sharper depletion of co-ions in the same region. This is due to increased electrostatic attractive and repulsive interactions of the membrane with counterions and co-ions, respectively. As the valence of the interfacial groups increases from $Z_h = 1$ to $Z_h = 4$, the accumulation of trivalent counterions is further enhanced due to increasing charge correlations. Moreover, it is the presence of multivalent interfacial groups that pushes the peak in the density profile of monovalent counterions back to the closest contact distance. On the other hand, the interionic association between counterions and co-ions also gives rise to an increment in the amount of adsorption of like-charged co-ions. As seen, our curves for all cases considered here show a crossover of counterion and co-ion density profiles. The crossover is an important symbol of charge inversion, and we will return in detail to this point later by means of the integrated charge distribution. In addition, the rise of Z_h in case of RPM representation results in a greater diffuse-layer width, in contrast to the same systems but for a weakly charged surface as evidenced in Figure 1. However, in the UPM approximation, we see a thinner EDL with an increase in the charge of

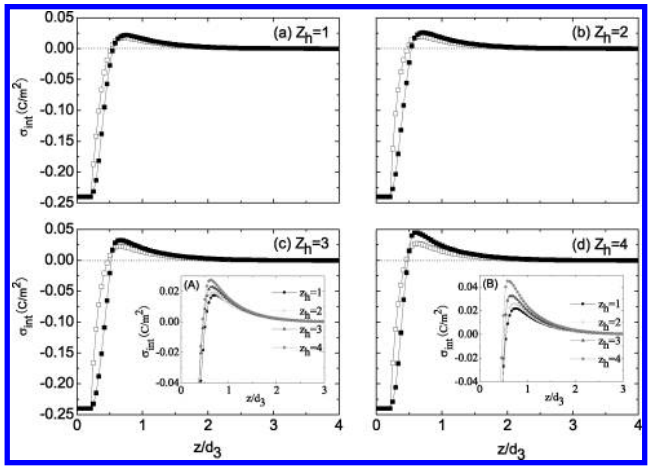

Figure 7. Integrated charge profiles plotted as a function of the dimensionless distance to the surface within the framework of the RPM approximation. All parameters are the same as in Figure 5. Open and solid symbols represent the results in the absence and presence of dielectric images, respectively. Insets: Magnification of integrated charge at small values of interfacial distance for varying valence of the head groups in the (A) absence and (B) presence of dielectric images.

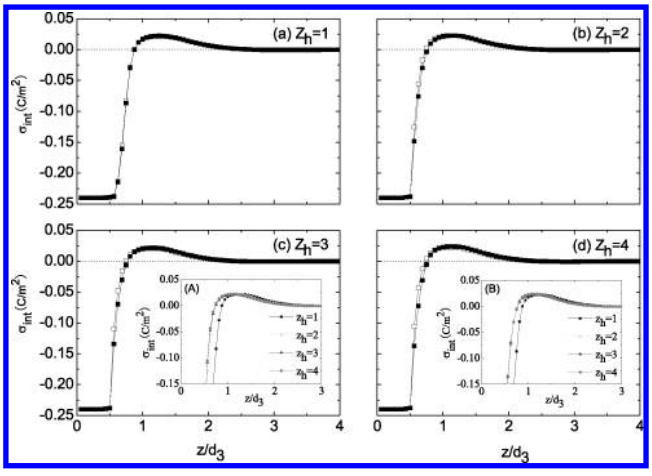

Figure 8. Same as Figure 7 but for the UPM systems. All parameters are the same as in Figure 6.

interfacial groups, irrespective of the surface charge density. These comparisons signify that the interplay of both steric effects and interionic correlations has phenomenal influence on the double layer characteristics.

When taking account of dielectric discontinuities, we observe that image-charge repulsion still exerts an important influence on the structure of double layer at this high surface charge density for the RPM systems of small ionic diameters, though this effect becomes less striking visually as compared to the weakly charged surface before. For the UPM systems, on the other hand, the density profiles of ionic species are almost identical in the absence and presence of dielectric images. This means that the larger-sized ions lead to effective reduction of the depletion effect arising from dielectric jump, similar to the weak electrostatic coupling systems.

To describe the process that electrolyte ions gradually neutralize the fixed charges on the membrane, in Figures 7 and 8 we display variations of the integrated charge density distribution function from the charged surface into the bulk solution for the same systems considered in Figures 5 and 6. In both cases of the RPM and UPM representations, the integrated charge $\sigma_{int}(z)$ becomes positive in certain ranges of z, indicating the occurrence of charge inversion. This is because the charged surface in the aqueous solution strongly binds so many counterions that the sign of its native charge becomes inverted. The overscreening phenomenon might also be responsible for the attraction between two colloidal particles with surface charge densities of the same sign but dissimilar magnitude.[13−25] Upon inducing polarization charges, the onset of charge inversion is shifted to larger z in all four values of charge of interfacial groups, oppositely to the case of the weakly charged surface. However, for the RPM approximation as shown in Figure 7, the presence of dielectric images still enhances the degree of charge inversion. The situation is more apparent especially for $Z_h = 4$. A similar trend of variation is also observed for the same systems but at $\sigma_0 = -0.04$ C/m^2; see Figure 3. From the comparison between Figures 4 and 8, one can find that the higher surface charge densities in the UPM systems cancel surface charge amplification appearing in the characteristic region that is delimited by the contact planes of monovalent and trivalent species. This shows that surface charge amplification is anticipated to take place only at very low values of interfacial charge density, being consistent with the recent results for the situation of continuously distributed charge on the surface of colloidal particles.[44,49,50]

Additionally, one can observe from the insets of Figure 7 that the increase of the valence of interfacial groups causes the onset of charge inversion to gradually move toward the surface. Moreover, the increased Z_h value also leads to a monotonic increase in the magnitude of charge inversion, regardless of dielectric images. This trend of variation can first be detected in terms of the density curves of ionic species where the maximum of co-ion profile increases and the minima of counterion profiles deepens with the individual charge of interfacial groups. Please note that the situation is different from that at the low surface charge density of $\sigma_0 = -0.04$ C/m^2, where, when the image effects are present, a nonmonotonic variation occurs in the extremum of the integrated charge. Our data also imply that there must be a certain threshold of surface charge density to connect to the transition. This difference can be interpreted by the electrostatic coupling intensity that is directly proportional to the surface charge density.[13,14] That is, the strong coupling system yields more effective screening of the surface charges under the same conditions. The corresponding magnification of the integrated charge for the UPM representation of large-sized ions is depicted in the insets of Figure 8 for different valences of interfacial groups. It is easy to see that, although the onset of charge inversion also approaches the surface with the increase of Z_h, some sort of saturation appears for multivalent interfacial groups. This feature is irrelevant to dielectric discontinuities. In addition, the extremum of the integrated charge remains almost invariant for all cases under study, which is similar to the weakly charged surface.

IV. Concluding Remarks

An extensive series of Monte Carlo simulations of mixed electrolyte solutions of 1:1 and 3:1 salts both with the same bulk concentration of 100 mM near a negatively charged planar interface at ambient conditions have been performed and analyzed using the primitive model by means of ionic density profiles and the integrated charge curves. The system was investigated by varying the number of parameters such as ionic sizes and asymmetry of ion sizes, individual charge of interfacial groups, dielectric images and surface charge density.

The main highlights of our results are emphasized as follows: For the weakly charged surface, the increasing excluded volume

gives rise to increased attraction between the surface charges and the counterions in the absence of dielectric images. Hence, the effective screening is caused by the high degree of counterion binding, yielding stronger charge inversion. This behavior is quite similar to the case of a continuous distribution of surface charges. In particular, we observe that, in the RPM approximation, where small-sized ions are taken into account, the amount of charge inversion increases monotonically with the charge of interfacial groups. By polarizing the membrane surface, the presence of multivalent interfacial groups further raises the magnitude of charge inversion regardless of drastic image repulsion but the monotonic behavior is not reproduced. As the ionic size increases, however, the peak in the integrated charge reflecting the degree of charge inversion is less sensitive to the valence of interfacial groups and remains almost equal in the height in the absence and presence of electrostatic images. Rather unexpectedly, when the valence of interfacial groups is taken to be 4, charge inversion becomes stronger in the RPM than in the UPM as long as dielectric images are considered. This observation provides robust evidence against the traditional view that larger ions always screen the surface charges more effectively. Similar findings except that the amount of charge inversion increases monotonically in the presence of dielectric images can be appreciated for the highly charged surface, notwithstanding to a relatively weakened degree. Overall, our results show that the enhancement of charge inversion by multivalent interfacial groups is dominated to a great extent by the sizes of charged species in the solution. Quite interesting, if the co-ions are smaller than the counterions, surface charge amplification is observed at low surface charge density whose magnitude is gradually increased with the augment of individual charge of the interfacial groups. Note also that surface charge amplification occurring in our UPM systems may well be eliminated if the interfacial charges are continuously distributed on the membrane, indicating the importance of the structure of the interfacial groups.

In addition, it has been shown that, depending on the surface charge density, the presence of dielectric images causes that the onset of charge inversion shifts either closer to or farther from the interface relative to the no-image case. This process of variation is intimately linked to the values of charge of interfacial groups but becomes less pronounced when the diameters of all the ionic components in the bulk solution are increased. At any rate, our simulations reveal that the intricate interplay between steric and charge correlations has significant impact on the double layer characteristics. We hope that our work will serve as a foundation for future contributions on the development of theoretical methods through considering more realistic factors to explain charge inversion more quantitatively.

Acknowledgment. This work was supported by the National Basic Research Program of China (No. 2007CB925101) and the National Natural Science Foundation of China (Nos. 10974080, 20674037, and 10629401). Z.W. gratefully thanks the Doctorial Start-up Fund of Chongqing University of Technology. We are grateful to the High Performance Computing Center of Nanjing University for doing the numerical calculations in this paper on its IBM Blade cluster system.

References and Notes

(1) Evans, D. F.; Wennerström, H. *The Colloidal Domain: Where Physics, Chemistry, Biology, and Technology Meet*, 2nd ed.; Wiley-VCH: New York, 1999.
(2) Holm, C.; Kekicheff, P.; Podgornik, R. *Electrostatic Effects in Soft Matter and Biophysics*; Kluwer Academic Publishers: Dordrecht, The Netherlands, 2001.
(3) Attard, P. *Adv. Chem. Phys.* **1996**, *92*, 1.
(4) Strauss, U. P.; Gershfeld, N. L.; Spiera, H. *J. Am. Chem. Soc.* **1954**, *76*, 5909.
(5) Kirkwood, J. G.; Shumaker, J. B. *Proc. Natl. Acad. Sci. U.S.A.* **1952**, *38*, 863.
(6) Gelbart, W. M.; Bruinsma, R. F.; Pincus, P. A.; Parsegian, V. A. *Phys. Today* **2000**, *53*, 38.
(7) Lyklema, J. *Colloids Surf., A* **2006**, *291*, 3.
(8) Martín-Molina, A.; Calero, C.; Faraudo, J.; Quesada-Pérez, M.; Travesset, A.; Hidalgo-Álvarez, R. *Soft Matter* **2009**, *5*, 1350.
(9) Faraudo, J.; Travesset, A. *J. Phys. Chem. C* **2007**, *111*, 987.
(10) Martín-Molina, A.; Rodríguez-Beas, C.; Faraudo, J. *Phys. Rev. Lett.* **2010**, *104*, 168103.
(11) Messina, R.; González-Tovar, E.; Lozada-Cassou, M.; Holm, C. *Europhys. Lett.* **2002**, *60*, 383.
(12) Wernersson, E.; Kjellander; Lyklema, J. *J. Phys. Chem. C* **2010**, *114*, 1849.
(13) Grosberg, A. Y.; Nguyen, T. T.; Shklovskii, B. I. *Rev. Mod. Phys.* **2002**, *74*, 329.
(14) Levin, Y. *Rep. Prog. Phys.* **2002**, *65*, 1577.
(15) Quesada-Pérez, M.; González-Tovar, E.; Martín-Molina, A.; Lozada-Cassou, M.; Hidalgo-Álvarez, R. *ChemPhysChem* **2003**, *4*, 234.
(16) Naji, A.; Netz, R. R. *Eur. Phys. J. E* **2004**, *13*, 43.
(17) Israelachvili, J. N.; McGuiggan, P. M. *Science* **1988**, *241*, 795.
(18) Larsen, A. E.; Grier, D. G. *Nature* **1997**, *385*, 230.
(19) Deserno, C.; Holm, C.; May, S. *Macromolecules* **2000**, *33*, 199.
(20) Zohar, O.; Leizerson, I.; Sivan, U. *Phys. Rev. Lett.* **2006**, *96*, 177802.
(21) Parsegian, V. A.; Rand, R. P.; Rau, D. C. *Proc. Natl. Acad. Sci. U.S.A.* **2000**, *97*, 3987.
(22) Bowen, W. R.; Sharif, A. O. *Nature* **1998**, *393*, 663.
(23) Popa, I.; Gillies, G.; Papastavrou, G.; Borkovec, M. *J. Phys. Chem. B* **2009**, *113*, 8458.
(24) Bloomfield, V. A. *Curr. Opin. Struct. Biol.* **1996**, *6*, 334.
(25) Angelini, T. E.; Liang, H.; Wriggers, W.; Wong, G. C. L. *Proc. Natl. Acad. Sci. U.S.A.* **2003**, *100*, 8634.
(26) Kabanov, A. V.; Kabanov, V. A. *Adv. Drug Delivery Rev.* **1998**, *30*, 49.
(27) Gössl, I.; Shu, L.; Schlüter, A. D.; Rabe, J. P. *J. Am. Chem. Soc.* **2002**, *124*, 6860.
(28) Rädler, J. O.; Koltover, I.; Salditt, T.; Safinya, C. R. *Science* **1997**, *275*, 810.
(29) Nel, A. E.; Mädler, L.; Velegol, D.; Xia, T.; Hoek, E. M. V.; Somasundaran, P.; Klaessig, F.; Castranova, V.; Thompson, M. *Nat. Mater.* **2009**, *8*, 543.
(30) Lynch, I.; Cedervall, T.; Lundqvist, M.; Cabaleiro-Lago, C.; Linse, S.; Dawson, K. A. *Adv. Colloid Interface Sci.* **2007**, *134*−*135*, 167.
(31) Yoo, P. J.; Nam, K. T.; Qi, J.; Lee, S.-K.; Park, J.; Belcher, A. M.; Hammond, P. T. *Nat. Mater.* **2006**, *5*, 234.
(32) Kind, M.; Wöll, C. *Prog. Surf. Sci.* **2009**, *84*, 230.
(33) Cooper, G. M. *The Cell: A Molecular Approach*; ASM Press: Washington, DC, 2000.
(34) Haleva, E.; Ben-Tal, N.; Diamant, H. *Biophys. J.* **2005**, *86*, 2165.
(35) Faraudo, J.; Travesset, A. *Biophys. J.* **2007**, *92*, 2806.
(36) Tzlil, S.; Murray, D.; Ben-Shaul, A. *Biophys. J.* **2008**, *95*, 1745.
(37) Fleck, C.; Netz, R. R.; von Grünberg, H. H. *Biophys. J.* **2002**, *82*, 76.
(38) Calero, C.; Faraudo, J. *Phys. Rev. E* **2009**, *80*, 042601.
(39) Calero, C.; Faraudo, J. *J. Chem. Phys.* **2010**, *132*, 024704.
(40) Toghraee, R.; Mashl, J.; Lee, K.; Jakobsson, E.; Ravaioli, U. *J. Comput. Electron.* **2009**, *8*, 98.
(41) Lear, J. D.; Schneider, J. P.; Kienker, P. K.; DeGrado, W. F. *J. Am. Chem. Soc.* **1997**, *119*, 3212.
(42) Yaroshchuk, A. E. *Adv. Colloid Interface Sci.* **2000**, *85*, 193.
(43) Torrie, G. M.; Valleau, J. P.; Patey, G. N. *J. Chem. Phys.* **1982**, *76*, 4615.
(44) Wang, Z. Y.; Ma, Y. Q. *J. Chem. Phys.* **2009**, *131*, 244715.
(45) Henderson, D.; Gillespie, D.; Nagy, T.; Boda, D. *Mol. Phys.* **2005**, *103*, 2851.
(46) Tulpar, A.; Ducker, W. A. *J. Phys. Chem. B* **2004**, *108*, 1667.
(47) Allen, M. P.; Tildesley, D. J. *Computer Simulation of Liquids*; Oxford University Press: New York, 1987.
(48) Grzybowski, A.; Bródka, A. *Mol. Phys.* **2002**, *100*, 1017.
(49) Wang, Z. Y.; Ma, Y. Q. *J. Chem. Phys.* **2010**, *133*, 064704.
(50) Guerrero-García, G. I.; González-Tovar, E.; Olvera de la Cruz, M. *Soft Matter* **2010**, *6*, 2056.

JP106118Q